Fabrication and structural property of diamond nano-platelet arrays on {111} textured diamond film

Wei-Lin Wang *, Sheng-Ming Wang, Shih-Yin Cho, Li Chang

Department of Materials Science and Engineering, National Chiao Tung University, Hsinchu, Taiwan ROC

ARTICLE INFO

ABSTRACT

Diamond nano-platelet (DNP) arrays have been grown on {111} textured diamond film by using micro-wave plasma enhanced chemical vapor deposition system. Scanning electron microscopy (SEM) and transmission electron microscopy (TEM) have been used to characterize the growth behavior and micro-structure of DNP arrays on diamond film. According to the results of SEM and TEM images, DNP arrays only appear on the {111} surfaces of underlying diamond grains. Both DNPs and underlying diamond grains comprise penetration {111} twin structures. The growth of DNPs is the extension of the penetration {111} twins from underlying diamond grains. The accommodation and glide of stacking faults can also evolve into perfect {111} twin structures during the growth of DNPs.

© 2012 Elsevier B.V. All rights reserved.

1. Introduction

Recently, nano-crystalline materials with noticeable physical characteristics have been intensively studied. The synthesis of diamond in various nano-structures has drawn much attention for the application of field emission owing to its high breakdown field, chemical inertness, and the negative electron affinity with low work function [1,2]. Many studies have demonstrated the fabrication of diamond nano-tips and -whiskers or diamond-coated nano-wires on silicon (Si) substrate for field emitters [3–7]. In our previous report, diamond nano-platelets (DNPs) were also realized to perform a considerable field emission characteristic due to its specific geometric configuration with high aspect ratio [8]. Although DNPs can be successfully grown, the random distribution of DNPs as emission sites gives difficulty in high emission intensity. Therefore, the fabrication of regular DNP arrays on diamond film is more desirable.

Diamond film grown by chemical vapor deposition (CVD) is usually rough and poly-crystalline with large grains. For a diamond grain, the high density of {111} twins was observed. Nevertheless, those {111} twins were not parallel to {111} surfaces but parallel to other planes of {111} family, which presented penetration behavior in the diamond grain [9,10]. Interestingly, DNPs were also found to consist of multiple penetration {111} twins. Moreover, DNPs showed a growth direction parallel to the multiple {111} twin boundaries [11]. The penetration property of {111} twins in both DNPs and

diamond grains has given a great opportunity for the synthesis of DNP arrays and diamond film.

In this study, DNP arrays have been successfully fabricated on {111} textured diamond film by utilizing the penetration and extension of diamond {111} twins. Further, the growth mechanism and structural property of DNPs on diamond film have also been systematically investigated by employing scanning electron microscopy (SEM) and transmission electron microscopy (TEM).

2. Experimental procedure

A microwave plasma enhanced CVD system equipped with 1.5 kW microwave generator was used for the deposition of diamond film and the fabrication of DNP arrays. In order to obtain diamond film with large grain size in {111} texture as a template, (111)Si with the size of $1 \times 1 \, cm^2$ was chosen to be the substrate. The diamond film was grown at 700 W for 5 h with a pressure of 40 torr. The gas flow rates of CH_4 and H_2 were 0.4 and 200 sccm. The growth temperature was kept within 900–950 °C. For the fabrication of DNP arrays, the plasma power and growth temperature were increased to 1 kW and 1100 °C with a pressure of 20 torr. The flow rates were 14 and 500 sccm for CH_4 and H_2, respectively. The growth time was 10 min.

A JEOL-6700 field emission SEM was applied to examine the surface morphologies of {111} textured diamond film and DNP arrays. The growth behavior and structural property of DNPs on diamond film were investigated by using a JEOL 2100 F field emission TEM. The preparation of cross-sectional TEM (XTEM) specimen was carried out using standard mechanical grinding process and Ar$^+$ ion milling. The ion milling was accomplished in a Gatan Model 691 PIPS system. For unambiguous comprehension to the growth behavior and micro-structure of DNPs on diamond

---

* Corresponding author at: 1001, Tahsueh Road, Department of Materials Science and Engineering, National Chiao Tung University, Hsinchu, Taiwan 300. Tel.: +886 3 5731615; fax: +886 3 5724727.
E-mail address: wwelin@gmail.com (W.-L. Wang).

grain, the XTEM specimen was ground along $[10\bar{1}]$diamond for the viewing direction to be parallel to (111)diamond in XTEM observations.

3. Results and discussion

The surface morphology of pre-deposited diamond film on (111)Si substrate is shown by the SEM image in Fig. 1(a). The surface of the diamond film is almost covered by triangular {111} surfaces. The inset of Fig. 1(a) presents the image of {111} surfaces with higher magnification. Fig. 1(b) shows the top-view SEM image of DNPs grown on the diamond film. Apparently, DNPs only appear on triangular {111} surfaces. The neighboring facets of {111} surfaces marked by arrows are smooth without DNPs. Fig. 1(c) exhibits the DNPs grown on a diamond grain. Black solid lines draw the geometric relationships between the DNPs and the underlying triangle. The post-grown DNPs are parallel to three edges of the underlying {111} surface to form a regular array. The thickness of DNPs is around 17–25 nm.

In order to clarify the micro-structure of DNPs grown on a diamond grain, the bright-field XTEM (BF-XTEM) image observed along the $[10\bar{1}]$ direction of diamond is given in Fig. 2(a). As marked by dashed arrow in Fig. 1(c), the viewing direction of XTEM images is parallel to an edge of the underlying (111) surface. In Fig. 2(a), the residual G1
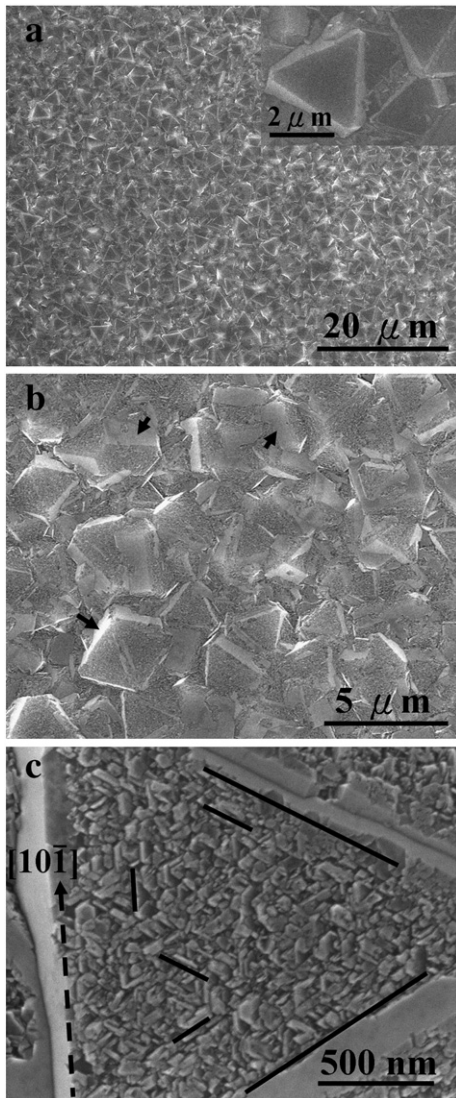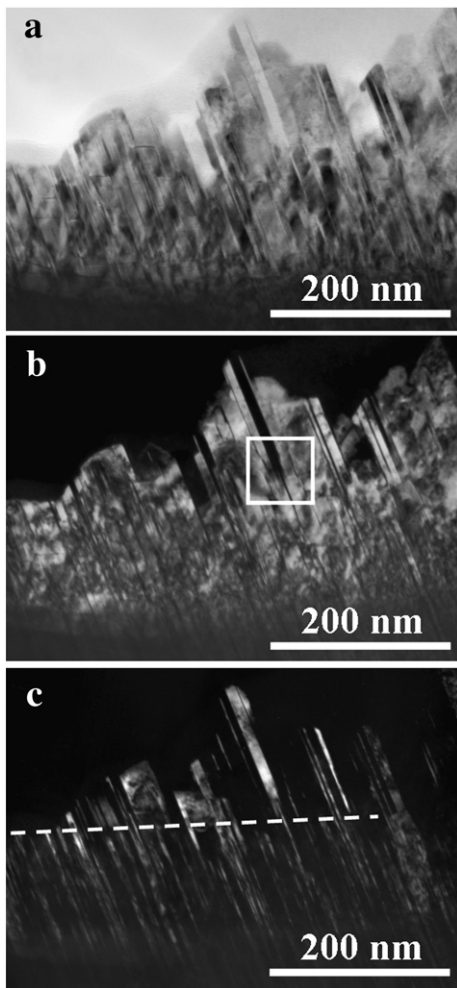

Fig. 1. (a) Top-view SEM image of {111} textured diamond film. The inset is a higher magnification image showing triangular facets. Top-view SEM images of (b) DNP arrays on {111} textured diamond film and (c) a single triangular surface with DNPs.

glue proves that the morphology of DNPs is original without damage from ion-milling. Fig. 2(b) shows the selected area diffraction (SAD) pattern taken from Fig. 2(a). The SAD pattern is identified to be under $[10\bar{1}]_{D1}$ and $[\bar{1}01]_{D2}$ zone axes. As encircled by solid and dashed lines, the SAD pattern comprises two groups of diffraction spots with mirror relation and the sharing of $\pm(\bar{1}1\bar{1})_{D1}$ and $\pm(1\bar{1}1)_{D2}$ diffraction spots. The result of the SAD pattern indicates that DNPs/diamond system consists of $(\bar{1}1\bar{1})$ twin structures, in which crystal diamond 1 and 2 are designated to be D1 and D2. For the identification of the interface between DNPs and underlying diamond grain, the comparison of SEM image, SAD pattern, and BF-XTEM image is required. As shown in Fig. 1(c), DNPs are not observed on the edges of the underlying triangular surface. According to the observation orientation relationship with Fig. 1(c), the left edge of the underlying surface should remain clear without DNPs in the XTEM image of Fig. 2(a). The smooth edge without DNPs can be regarded as the original (111) surface of the underlying diamond grain. Reasonably, the position of the original (111) surface is supposed to be the interface between DNPs and underlying diamond grain. Based on the crystal orientation defined by the $(111)_{D1}$ diffraction spot in the SAD pattern of Fig. 2(b), the diffracted $(111)_{D1}$ plane, parallel to the black-dashed line in Fig. 2(a), is also parallel to the smooth edge. Therefore, the black-dashed line hereby indicates the interface position. In Fig. 2(a), the $(010)_{D1}$ plane drawn by white-solid line is the neighboring facet of (111) surface which can be referred to those smooth facets without DNPs in the SEM image of Fig. 1(b). The higher magnification BF-XTEM image of DNPs is shown in Fig. 2(c). Black arrows point to the contrast of the $(\bar{1}1\bar{1})$ twin structures in DNPs. From the measurement in TEM images, the height of DNPs is about 150–200 nm.

To further comprehend the structural relationship between DNPs and underlying diamond grain, Fig. 3(a)–(c) exhibit BF-XTEM and dark-field XTEM (DF-XTEM) images, showing the same area for inspection and comparison. Fig. 3(a) is the BF-XTEM image taken under $[10\bar{1}]_{D1}$ and $[\bar{1}01]_{D2}$ zone axes. Fig. 3(b) and (c) obtained by selecting the $(111)_{D1}$ and $(111)_{D2}$ diffraction spots in Fig. 2(b), respectively, reveal crystal D1 and D2 in striped bright contrast. In Fig. 3(c), the dashed line represents the interface between DNPs and underlying diamond grain. In DF-XTEM images, highly dense multiple twins or micro-twins are observed in both DNPs and underlying diamond grain. The $(\bar{1}1\bar{1})$ twin structures of underlying diamond grain obviously propagate through the interface in the manner of homo-epitaxial relationship. The growth direction of DNPs is parallel to $(\bar{1}1\bar{1})$ twin boundaries. On the other hand, the newly-grown DNPs can be considered as the extension of the penetration twins from underlying diamond grain.

Fig. 4(a) is the high resolution XTEM (HR-XTEM) image taken from the dashed-square area in Fig. 2(c). In the HR-XTEM image, the perfectly coherent $(\bar{1}1\bar{1})$ twin structures are observed in the terminal part of DNP. Black-dashed lines define $(\bar{1}1\bar{1})$ twin boundaries in the DNP. White-solid lines depict (111) planes in each diamond crystal. The inset is the corresponding fast Fourier transform (FFT) pattern of the DNP. The FFT pattern also exhibits two groups of spots, because of $(\bar{1}1\bar{1})$ twin structures. In Fig. 4(a), the facets of the DNP terminal are identified to be a serial facets of (010)D1/(111)D2/(111)D1/(010)D2. The ridge edge of DNP terminal has been observed and discussed in the case of DNPs grown on nano-crystalline diamonds [11,12]. In Fig. 4(b), the HR-XTEM image photographed from the solid-square area in Fig. 2(c) shows the micro-structure near the interface region between DNPs and diamond grain. This region is the initial stage of DNP growth. The inset of Fig. 4(b) is the corresponding FFT pattern. In contrast to the FFT of Fig. 4(a), the FFT pattern of Fig. 4(b) displays the extra spots marked by circles, except the spots caused by $(\bar{1}1\bar{1})$ twin structures. In the matter of fact, the periodically extra diffraction spots at one-third $g=\bar{1}1\bar{1}$ are observed in the SAD pattern of Fig. 2(b) as well.

In diamond structure, the predominant crystal defects are not only {111} twins but also stacking faults with $1/6<1\bar{2}1>$ displacement
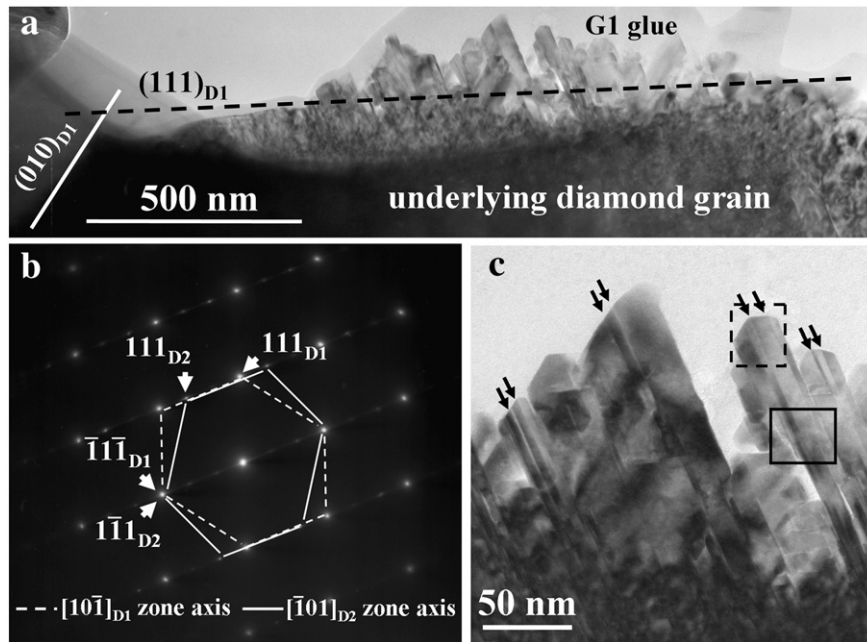
Fig. 2. (a) BF-XTEM image of DNPs grown on a diamond grain and (b) its corresponding SAD pattern. (c) BF-XTEM image of DNPs with higher magnification.

vectors gliding on {111} [9,13,14]. The diffuse intensity in between diffraction spots (and FFT spots) along $g = \bar{1}1\bar{1}$ is attributed to the existence of dense stacking faults indicated by white arrows in Fig. 4(b). In SAD and FFT patterns, the extra spots at the positions of one-third $g = \bar{1}1\bar{1}$ are the consequence of specific stacking

Fig. 3. (a) BF-XTEM image taken under $[10\bar{1}]_{D1}$ and $[\bar{1}01]_{D2}$ zone axes. (b) and (c) DF-XTEM images taken by selecting the diffraction spots of $(111)_{D1}$ and $(111)_{D2}$ showing crystal D1 and D2, respectively.
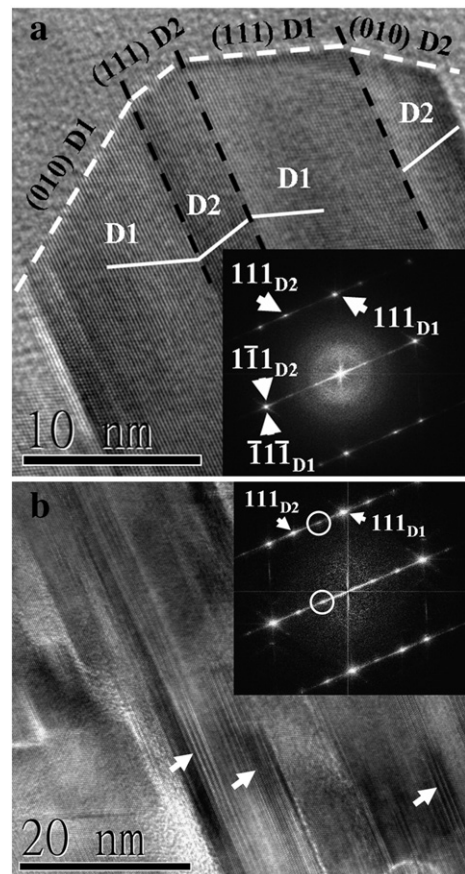
Fig. 4. HR-XTEM images of (a) the terminal of DNP and (b) the initial region of DNP. The insets in (a) and (b) are corresponding FFT patterns.
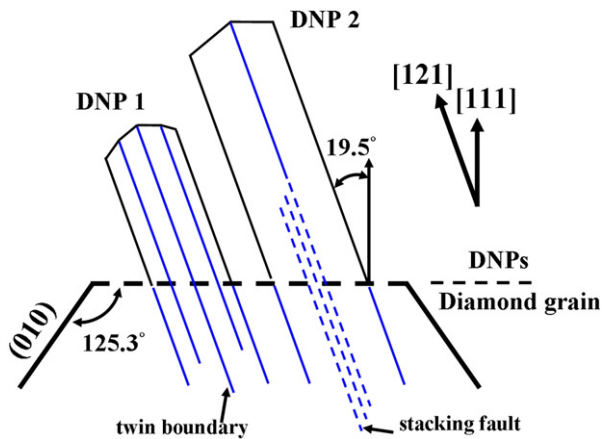
Fig. 5. Schematic representation of the growth mechanism and structural property for DNPs on diamond grain with the viewing direction of $[10\bar{1}]$. (The coordinate system and index in accordance with the orientation of D1 in Fig. 2).

structure. In perfect cubic diamond structure, the stacking sequence along <111> is ABCABCABC. By the intersections of stacking faults and multiple twins, the stacking sequence of ABCABCABC can be transformed into ABABAB which is regarded as hexagonal diamond structure [15,16]. The stacking structure of hexagonal diamond coincides with the structure of stacking fault arrangement in every three {111} interspacing. Therefore, the hexagonal diamond structures induced by defects are responsible for the spots arising at the position of one-third $g = \bar{1}1\bar{1}$. Furthermore, stacking faults are capable of inducing the appearance of twins in addition to the formation of hexagonal diamond. From the results of XTEM, it is noticed that highly dense stacking faults could extend upward into DNPs due to homo-epitaxial behavior. Through the observations of the HR-XTEM images taken from DNP terminal and its initial stage, the accommodation transition of stacking faults during the growth of DNPs is realized as following. The conversion of stacking sequence from ABCABCABCABC to ABCABC/BCABC takes place when a stacking fault appears on {111}. In order to reduce the total energy of the crystal, stacking faults glide on {111} plane to further accommodate, and then the stacking sequence becomes ABCABC/B/A/BC. During the growth of DNP, the stacking sequence transforms into ABCAB/C/BACBA after a serial glide of stacking faults. Consequently, the coherent twin structures with the reduction of total energy form in the end parts of DNPs. The above-mentioned glide process also explains the phenomenon in the white square area of Fig. 3(b), in which the bi-crystal becomes larger and more integrated with smoothly sharp twin boundary along the growth direction of DNP.

Based on the observations from SEM and TEM images, the growth mechanism of DNPs on diamond grain can be schematically described in Fig. 5. Black-dashed line denotes the original (111) surface of diamond grain. Blue-solid lines represent the $(\bar{1}11)$ twin boundaries in DNP and underlying diamond grain. As sketched, DNPs only appear on the (111) surface of underlying diamond grain. The angle between the growth direction of DNPs and the normal of underlying (111) plane is 19.5°. For DNPs, the terminal edge is verified to be ridge morphology according to the result of HR-XTEM image. The growth behavior of DNP 1 is simply the concept of the penetration $(\bar{1}1\bar{1})$ twin structures of underlying diamond grain extending upward to form nano-platelet. For DNP 2, the glides of stacking faults are involved with the formation of twin. Blue-dashed lines represent the same type of stacking faults with a displacement vector parallel to $(\bar{1}1\bar{1})$ twin plane. The accommodation transition of stacking faults takes place during the growth of the DNP. Eventually, a perfect twin structure forms in the DNP.

4. Conclusions

DNP arrays have been fabricated on the {111} triangle surfaces of {111} textured diamond film. Both post-grown DNPs and underlying diamond grains consist of multiple parallel {111} twin structures. On the characteristic of homo-epitaxial relationship, the growth behavior of DNPs is confirmed to be the extension of penetration {111} twins from underlying diamond grains. Beyond the interface between DNPs and diamond grains, the accommodation and glide of stacking faults can also result in the appearance of perfect {111} twin structures during the growth of DNPs.

References

[1] F.J. Himpsel, J.A. Knapp, J.A. VanVechten, D.E. Eastman, Phys. Rev. B 20 (1979) 624.
[2] W. Zhu, G.P. Kochanski, S. Jin, Science 282 (1998) 1471.
[3] D.G. Walker, C.T. Harris, T.S. Fisher, J.L. Davidson, Diamond Relat. Mater. 14 (2005) 113.
[4] A. Wisitsora-at, W.P. Kang, J.L. Davidson, D.V. Kerns, Appl. Phys. Lett. 71 (1997) 3394.
[5] J.D. Jarvis, H.L. Andrews, C.A. Brau, B.K. Choi, J. Davidson, W.-P. Kang, Y.-M. Wong, J. Vac. Sci. Technol. B 27 (2009) 2264.
[6] E.-S. Baik, Y.-J. Baik, S.W. Lee, D. Jeon, Thin Solid Films 377 (2000) 295.
[7] Y.F. Tzeng, Y.-C. Lee, C.-Y. Lee, I.-N. Lin, H.-T. Chiu, Appl. Phys. Lett. 91 (2007) 063117.
[8] H.G. Chen, L. Chang, Diamond Relat. Mater. 18 (2009) 141.
[9] B.E. Williams, H.S. Kong, J.T. Glass, J. Mater. Res. 5 (1990) 801.
[10] Z.L. Wang, J. Benthley, R.E. Clausing, L. Heatherly, L.L. Horton, J. Mater. Res. 9 (1994) 1552.
[11] H.G. Chen, L. Chang, S.Y. Cho, J.K. Yan, C.A. Lu, Chem. Vap. Deposition 14 (2008) 247.
[12] H.G. Chen, L. Chang, J. Mater. Res. 20 (2005) 703.
[13] B.E. Williams, J.T. Glass, J. Mater. Res. 4 (1989) 373.
[14] S. Roy, M. Portail, T. Chassagne, J.M. Chauveau, P. Vennéguès, M. Zielinski, Appl. Phys. Lett. 95 (2009) 081903.
[15] U. Dahmen, K.H. Westmacott, R. Pirouz, R. Chaim, Acta Metall. Mater. 23 (1990) 269.
[16] H. He, T. Sekine, T. Kobayashi, Appl. Phys. Lett. 81 (2002) 610.